



HAL
open science

Resistance switching variability in HfO₂-based memory structures with different electrodes

Thomas Cabout, Julien Buckley, Carlo Cagli, Vincent Jousseau,
Jean-François Nodin, Barbara de Salvo, Marc Bocquet, Christophe Muller

► **To cite this version:**

Thomas Cabout, Julien Buckley, Carlo Cagli, Vincent Jousseau, Jean-François Nodin, et al.. Resistance switching variability in HfO₂-based memory structures with different electrodes. EMRS Spring Meeting 2012, May 2012, Strasbourg France. hal-01738395

HAL Id: hal-01738395

<https://hal.science/hal-01738395>

Submitted on 20 Mar 2018

HAL is a multi-disciplinary open access archive for the deposit and dissemination of scientific research documents, whether they are published or not. The documents may come from teaching and research institutions in France or abroad, or from public or private research centers.

L'archive ouverte pluridisciplinaire **HAL**, est destinée au dépôt et à la diffusion de documents scientifiques de niveau recherche, publiés ou non, émanant des établissements d'enseignement et de recherche français ou étrangers, des laboratoires publics ou privés.

Manuscript Number: TSF-D-12-01300

Title: Resistance switching variability in HfO₂-based memory structures with different electrodes

Article Type: EMRS 2012 Symposium L

Keywords: switching memory; HfO₂ switchable layer; titanium-based electrodes; variability

Corresponding Author: Mr Thomas Cabout,

Corresponding Author's Institution: CEA, LETI, MINATEC Campus

First Author: Thomas Cabout

Order of Authors: Thomas Cabout; Julien Buckley; Carlo Cagli; Vincent Jousseau; Jean-François Nodin; Barbara De Salvo; Marc Bocquet; Christophe Muller

Abstract: This paper deals with the effect of platinum or titanium-based electrodes on resistive switching characteristics and electrical performances of HfO₂-based memory elements. Capacitor-like Pt/HfO₂(10nm)/Pt and Ti/HfO₂(10nm)/TiN structures were fabricated on top of a tungsten pillar bottom electrode and integrated in-between two interconnect metal lines. Initially, quasi-static measurements were performed to study the influence of electrode nature on forming, set and reset operations and their corresponding switching parameters. Memory elements with top and bottom Pt electrodes exhibited a non-polar behavior with sharp decrease of current during reset operation while cells integrating Ti-based electrodes showed a bipolar switching behavior, with a progressive reset. Then, statistical distribution of switching parameters (voltage and resistance) were extracted from data obtained on hundreds of memory devices. Even if the resistance in the low resistive state (LRS) and the reset voltage were found to be comparable for both kinds of electrodes. On the other hand, the progressive reset operation observed on samples with Ti-based electrodes led to a lower variability of resistance in high resistive state (HRS) and subsequently of set voltage. In addition Ti-based electrodes enabled gaining: (i) lower forming and set voltages with significantly narrower cell-to-cell distributions; (ii) a better data retention (10 years at 65°C instead of 10 years at 50°C for Pt electrodes); (iii) satisfactory dynamic performances with lower set and reset voltages for ramp speed ranging from 10⁻² to 10⁷ V/s.

Suggested Reviewers: Gérard Ghibaudo
IMEP, IMEP-CNRS Minatec
ghibaudo@minatec.inpg.fr

Thierry BARON
LTM, CEA-LETI
thierry.baron@cea.fr

Andrea Padovani
DISMI, Università di Modena e Reggio Emilia
andrea.padovani@unimore.it

Extended paper on "Resistance switching variability in HfO₂-based memory structures with different electrodes" after oral presentation in E-MRS Spring meeting 2012 in Symposium L: Novel Functional Materials and Nanostructures for innovative non-volatile memory devices.

We study influence of electrode materials on switching behaviour.

We study influence of electrode materials on switching parameters variability.

Switching behaviours are link to switching parameters variability.

Data retention and dynamic performances are assessed.

Resistance switching variability in HfO₂-based memory structures with different electrodes

T. Cabout^a, J. Buckley^a, C. Cagli^a, V. Jousseume^a, J-F. Nodin^a, B. de Salvo^a,
M. Bocquet^b, Ch. Muller^b

^aCEA LETI, MINATEC Campus, Grenoble France

^bIm2np, UMR CNRS 7334, Aix-Marseille Université, Marseille France

Abstract

This paper deals with the effect of platinum or titanium-based electrodes on resistive switching characteristics and electrical performances of HfO₂-based memory elements. Capacitor-like Pt/HfO₂(10nm)/Pt and Ti/HfO₂(10nm)/TiN structures were fabricated on top of a tungsten pillar bottom electrode and integrated in-between two interconnect metal lines. Initially, quasi-static measurements were performed to study the influence of electrode nature on *forming*, *set* and *reset* operations and their corresponding switching parameters. Memory elements with top and bottom Pt electrodes exhibited a non-polar behavior with sharp decrease of current during *reset* operation while cells integrating Ti-based electrodes showed a bipolar switching behavior, with a progressive *reset*. Then, statistical distributions of switching parameters (voltage and resistance) were extracted from data obtained on hundreds of memory devices. Even if the resistance in the low resistive state (LRS) and the *reset* voltage were found to be comparable for both kinds of electrodes. On the other hand, the

progressive *reset* operation observed on samples with Ti-based electrodes led to a lower variability of resistance in high resistive state (HRS) and subsequently of *set* voltage. In addition Ti-based electrodes enabled gaining: (i) lower *forming* and *set* voltages with significantly narrower cell-to-cell distributions; (ii) a better data retention (10 years at 65°C instead of 10 years at 50°C for Pt electrodes); (iii) satisfactory dynamic performances with lower *set* and *reset* voltages for ramp speed ranging from 10^{-2} to 10^7 V/s.

1. Introduction

Flash memories, in the NAND (data memory – dense and cheap) or NOR (code memory – fast) architecture, are today the undisputed reference for the non-volatile memory market and applications. However, as the downscaling and cost reduction trend of conventional floating gate memories appears ever more complicated below the 20 nm technological node, opportunities are opened for alternative concepts. Among emerging technologies, Oxide Resistive Random Access Memory (OxRRAM) appears one of the most promising solutions for the next non-volatile memory generation. Based on a reversible voltage-controlled resistance change between high resistive state (HRS) and low resistive state (LRS), the simple capacitor-like Metal-Insulator-Metal (MIM) structure of OxRRAM offers suitable CMOS compatibility with possible integration into Back-End of Line (BEOL) interconnects. Besides, this technology attracts a particular interest for very high-density storage and paves the way to multilevel tri-dimensional architectures [1]. Excellent electrical performances in terms of low voltage operations [2], high programming speed [3] and long retention [4] were already demonstrated. However, OxRRAM concept is still in its infancy compared to other technologies and the cell-to-cell variability of switching parameters is still a very serious issue for future industrialization [5]. Regarding the switchable material, several metal oxides were

reported to exhibit voltage-controlled resistance change [6] and recently a growing interest was turned towards hafnium oxide (HfO_2) that undergoes a bipolar resistance switching. Beside the nature of switchable metal oxide, a peculiar attention must be paid to electrodes that may deeply modify the electrical behavior of MIM capacitors. In this context, this paper reports the electrical characteristics of two sets of capacitor-like structures integrating either Pt or Ti-based electrodes. The main aim is to apprehend the influence of electrodes on the switching parameters and the intrinsic cell-to-cell variability.

2. Experimental

2.1. Fabrication of capacitor-like structures

Memory elements were integrated into BEOL between metal lines noted M1 and M2 in Fig. 1. Capacitor-like MIM structures were fabricated on top of a tungsten pillar bottom plug (600 nm in diameter) connecting metal line M1. MIM capacitors consisted in a 10 nm thick HfO_2 oxide layer grown by Atomic Layer Deposition (ALD) at 350°C and sandwiched between two sputtered metallic electrodes. To apprehend the influence of electrode materials on switching characteristics two sets of devices were fabricated with either Pt (25 nm thick) as top and bottom electrodes (namely Pt/ HfO_2 /Pt structures) or Ti-based electrodes corresponding to Ti(10 nm)/ HfO_2 /TiN(25 nm) structures. Memory stacks were then etched to form MIM capacitors with a typical diameter of 1 μm . Finally a TiN-covering layer was deposited on top electrode to connect the second metal line M2. Note that the device architecture is called "1R", since it does not integrate an access transistor.

X-ray diffraction patterns recorded on HfO_2 blanket film showed that oxide layer crystallizes in a monoclinic symmetry when sandwiched with Pt electrodes while orthorhombic symmetry is favored by using Ti-based electrodes. Besides, composition profiles measured by Energy

Dispersive X-ray spectroscopy (EDX) revealed the formation of a layer at the interface Ti/HfO₂ due to O-getter character of titanium [8].

Fig. 1. Schematic representation of HfO₂-based memory elements in the form of capacitor-like MIM structures integrated between two metal lines noted M1 and M2. Memory stack is deposited on top of a tungsten pillar bottom electrode.

2.2. Electrical characterization

Quasi-static measurements were performed on devices to assess the electrical behavior and apprehend their switching characteristics at low voltage ramp speeds. Current-voltage (I-V) characteristics were measured with a standard parameter analyzer HP 4155 (Agilent Company), a current compliance of 1 mA being fixed for *forming* and *set* operations.

In complement, dynamic measurements were performed to evaluate electrical performances of MIM structures submitted to voltage pulses. The dependence of switching parameters on ramp speed was carefully studied for both *set* and *reset* operations with a pulse generator Agilent 81110A that enabled varying voltage ramps from 10⁻² to 10⁷ V/s.

3. Switching characteristics in quasi-static mode

3.1. Polarity assessment

Several *set* and *reset* cycles were applied to both sets of MIM structures to assess their electrical behavior, *i.e.* unipolar, bipolar or non-polar. Voltage was considered as positive when applied on top electrode. The split with Pt electrodes showed a versatile non-polar behavior: as shown on I-V characteristics in Fig. 2a, *set* operation was achievable for both voltage polarities and *reset* was possible in all polarities independently of the polarity used for preceding *set* operation. In contrast, MIM capacitors with Ti-based electrodes exhibited a

bipolar behavior: as depicted in Fig. 2b, *set* operation was possible only when a positive voltage was applied on top electrode and *reset* operation required the opposite polarity to switch back the memory element into a high resistance state.

Whatever the electrodes *set* operation from HRS to LRS was observed at a current level of about 10^{-5} A. In contrast, non-polar and bipolar behaviors were clearly distinguished for *reset* operation. Indeed, for capacitors with Pt electrodes *reset* operation was characterized by a sudden and sharp current drop towards a very high resistance state (average resistance of $4 \times 10^6 \Omega$). For Ti-based electrodes devices exhibiting a bipolar behavior, *reset* was progressive with gradual steps in the current decrease, this feature leading to smaller resistances in HRS ($5 \times 10^5 \Omega$). These latter observations are in favor of a thermal dissolution of conductive filaments proposed for non-polar/unipolar devices [9, 10] with drift-diffusion mechanisms described in [11].

For clarity and for a better comparison of switching parameters, in the following it was chosen to switch both sets of capacitors in a bipolar mode, *forming* and *set* operations being achieved with positive voltage while *reset* state was reached by applying negative voltage on top electrode.

Fig. 2. Depending on the nature of electrodes sandwiching HfO_2 layer, the switching behavior is either Non-polar behavior with Pt top and bottom electrodes (a) or bipolar with Ti-based electrodes.

3.2. Comparison of *forming* voltages

Forming operations were performed on more than 250 pristine capacitors, for each split of electrodes, by applying voltage ramp with a current compliance fixed to 1 mA. Nevertheless, due to the very fast switching the current compliance does not avoid current overshoot

occurring during *forming* stage. Tirano *et al.*[7] attributed this phenomenon to the discharge of a parasitic capacitance in parallel to the resistive device in simple 1R (one resistor, no transistor/diode selector) architectures [7]. Table 1 summarizes *forming* voltages (and their error bars) measured on both sets of capacitors. For samples relying on Ti-based electrodes it was observed significantly smaller *forming* voltages by a factor 2 as compared to capacitors with Pt electrodes (2 V instead of 4.3 V). This reduction of *forming* voltage was recently explained by the formation of an oxygen vacancies-rich TiO_x layer at the top interface Ti/HfO₂ [8]. This oxygen sub-stoichiometric layer enhances the defect-assisted conduction and contributes to decrease the effective thickness of switchable oxide layer.

Table 1. Summary of switching parameters extracted on the two sets of capacitors.

Capacitor- like structures	$V_{Forming}$ [V]	V_{Set} [V]	V_{Reset} [V]	R_{Set} [Ω]	R_{Reset} [Ω]
Pt/HfO ₂ /Pt	4.3 ± 0.6	2.5 ± 0.9	-0.38 ± 0.09	120	~4 M
Ti/HfO ₂ /TiN	2.0 ± 0.7	0.6 ± 0.4	-0.42 ± 0.06	480	~400 k

3.3. Cell-to-cell variability for *set* and *reset* operations

Several *set* and *reset* cycles (20 cycles) were systematically performed on more than 250 capacitors to apprehend the cell-to-cell variability. A summary of switching parameters is given in Table 1. First, regarding LRS-to-HRS *reset* operation, both sets of capacitors exhibited a switching at a negative voltage of about -0.4 V. Fig. 3a shows the cumulative cell-

to-cell distributions of *reset* voltages for both sets of electrodes: a low variability was observed which was not evidently influenced by the nature of electrodes. Since *reset* voltages were similar for both sets of MIM structures, the resistances in *set* state were subsequently close (Fig. 3b) and their variability comparable. This latter feature clearly indicates that R_{Set} and V_{Reset} were strongly correlated. Capacitors with Ti-based electrodes exhibited a slightly larger average resistance in *set* state of about 480 Ω instead of 120 Ω for cells with Pt electrodes.

HRS-to-LRS *set* operations were analysed as previously discussed. The cumulative distribution function of *set* voltages V_{Set} presented in Fig. 4a clearly shows that capacitors with Ti-based electrodes switched at a significantly lower voltage, typically 0.6 V instead of 2.5 V for structures with Pt as electrodes. Besides, it appears that the cell-to-cell variability was substantially narrower for Ti-based electrodes. This latter characteristic may be linked to the cell-to-cell variability observed on R_{Reset} resistance in HRS (Fig. 4b) for both sets of electrodes. One can observe a clear narrowing of variability for capacitors with Ti-based electrodes while Pt electrodes evidently led to a higher *reset* resistance with a significantly broader dispersion. This feature well matches the two types of *reset* operations observed for non-polar/unipolar and bipolar behaviors. As already mentioned, non-polar MIM capacitors with Pt electrodes exhibited a very sharp current decrease during *reset* operation that puts the cell in a very high resistance state. In contrast, bipolar capacitors with Ti-based electrodes showed a softer and progressive *reset* operation with several jumps in the current (*cf.* Fig. 2b) and a resulting lower resistance in HRS. Besides, the lower variability of R_{Reset} evidently demonstrated a better repeatability of *set* operations. Nevertheless, it should be noted that the lower resistance in HRS led to a closing of the programming window (*i.e.* R_{Reset}/R_{Set} ratio), decreasing from 8×10^5 to 7×10^2 for Pt and Ti-based electrodes, respectively.

To summarize, the different resistances in HRS have a noteworthy influence on *set* voltage. MIM capacitors with Ti-based electrodes exhibited a narrower cell-to-cell variability of lower *set* voltages V_{Set} linked to a thinner distribution of higher *reset* resistances R_{Reset} . In contrast, no correlation between distribution functions of V_{Reset} and R_{Set} may be straightforwardly done since *set* operation was certainly impacted by the current overshoot that may occur during switching [7]. 1T/1R devices are mandatory for a suitable control of *set* current.

Fig. 3. Cumulative cell-to-cell distribution functions for *reset* voltage (in absolute value) (a) and resulting resistance in *set* state (b). Distributions are given for MIM capacitors integrating either Pt (blue) or Ti-based (red) electrodes.

Fig. 4. Cumulative cell-to-cell distribution functions for *set* voltage (a) and resulting resistance in *reset* state (b). Distributions are given for MIM capacitors integrating either Pt (blue) or Ti-based (red) electrodes.

3.4. Data retention

Data retention were estimated by measuring the time-to-failure from either LRS or HRS state at different temperatures. Whatever the electrodes, HRS state was found to be highly stable since no failure was observed after 10 hours at 300°C. In contrast, LRS appeared unstable with failures observed at high temperature. To have a better insight on LRS retention capability, time-to-failure was measured as MIM structures were heated at different temperatures. Memory cells functionality at high temperature were firstly checked by performing *forming*, *reset* and *set* operations at test temperature. Cells were then programmed in LRS state and their resistance was subsequently measured as a function of time. As shown in inset of Fig. 5, the time-to-failure was determined when resistance reached 10 times the

initial LRS resistance. Results for different test temperatures are displayed in the form of an Arrhenius plot shown in Fig. 5. This latter plot is in good agreement with behavior generally observed on OxRRAM cells [12] and demonstrates better retention capabilities for MIM structures with Ti-based electrodes. The extrapolation to 10 years enabled us estimating 65°C as retention temperature for Ti-electrode structures against 50°C for Pt electrode structures. Hence, Ti-based electrodes sandwiching HfO₂ oxide layer enable improving data retention capabilities.

Fig. 5. Temperature-dependent Arrhenius plot of time-to-failure for both sets of electrodes. Extrapolation to 10 years enables extracting the retention temperature (10 years retention at 65°C for MIM capacitors with Ti-based electrodes). Inset shows time dependent evolution of resistance that enables determining the time-to-failure corresponding to LRS-to-HRS switching.

4. Dynamic characterization

As shown in the inset of Fig. 6a, experimental setup associated a load resistance in series with device under test. Applied voltage V_{Appl} and voltage across OxRRAM device V_{Cell} were monitored during operations to determine the switching voltages V_{Set} and V_{Reset} . Fig. 6a presents *set* operation achieved as capacitor was submitted to a triangular voltage pulse. Switching was detected by a sudden variation of V_{Cell} induced by the resistance change that modifies the ratio of the voltage divider formed by load resistance and OxRRAM resistance. Ramp speed dependence of *set* and *reset* voltages was measured on both sets of MIM structures (Fig. 6b). Accordingly with quasi-static measurements previously described, *set* and *reset* voltages and their associated variability were shown to be significantly lower for

capacitors integrating Ti-base electrodes, with V_{Set} and $|V_{Reset}|$ below 1 V even at 10^7 V/s (*i.e.* 0.7 V at 8×10^6 V/s). In contrast, MIM capacitors with Pt electrodes exhibited higher voltages with larger dispersions. Consequently, Ti-based electrodes incontestably enabled improving dynamic performances with *set* and *reset* operations achieved below 1 V (in absolute values).

Fig. 6. (a) Triangular applied voltage pulse V_{Appl} for dynamically measuring *set* voltage V_{Set} . Experimental setup is shown in the inset. (b) Ramp speed dependence of *set* and *reset* voltages for the two sets of capacitors integrating either Pt electrodes (blue) or Ti-based electrodes (red).

5. Conclusions

This paper compared switching characteristics and cell-to-cell variability of MIM structures relying on HfO₂ oxide layer sandwiched by either platinum or titanium-based electrodes. Capacitor-like structures were deposited on top of a tungsten pillar plug and integrated in-between two interconnect metal lines. Quasi-static and dynamic measurements clearly demonstrated better performance for structures with Ti-based electrodes, *i.e.*: (i) lower variability of resistance in high resistive state (HRS), and subsequently of *set* voltage; (ii) lower *forming* and *set* voltages with significantly narrower cell-to-cell distribution; (iii) a improved data retention (10 years at 65°C, instead of 50°C for Pt electrodes); (iv) satisfactory dynamic performances with lower *set* and *reset* voltages for ramp speed ranging from 10^{-2} to 10^7 V/s.

References

- [1] Ch. Muller, D. Deleruyelle, O. Ginez, “Emerging Memory Concepts: Materials, Modeling and Design”, In “Design Technology for Heterogeneous Embedded Systems”, Edited by G. Nicolescu, I. O’Connor, C. Piguet, Springer, Chapter 16, pp. 339–364, 2011 (ISBN 978-94-007-1124-2)
- [2] B. Govoreanu, G.S. Kar, Y.-y Chen, V. Paraschiv, S. Kubicek, A. Fantini, I.P. Radu, L. Goux, S. Clima, R. Degraeve, N. Jossart, O. Richard, T. Vandeweyer, K. Seo, P. Hendrickx, G. Pourtois, H. Bender, L. Altimime, D.J. Wouters, J.A. Kittl, M. Jurczak, B.- Leuven, K.U. Leuven, in:, 2011 IEEE International Electron Devices Meeting (IEDM), 2011, pp. 729-732.
- [3] Y.S. Chen, H.Y. Lee, P.S. Chen, P.Y. Gu, C.W. Chen, W.P. Lin, W.H. Liu, Y.Y. Hsu, S.S. Sheu, P.C. Chiang, W.S. Chen, F.T. Chen, C.H. Lien, M.-J. Tsai, 2009 IEEE International Electron Devices Meeting (IEDM) (2009) 1-4.
- [4] Z. Wei, Y. Kanzawa, K. Arita, Y. Katoh, K. Kawai, S. Muraoka, S. Mitani, S. Fujii, K. Katayama, M. Iijima, T. Mikawa, T. Ninomiya, R. Miyanaga, Y. Kawashima, K. Tsuji, a. Himeno, T. Okada, R. Azuma, K. Shimakawa, H. Sugaya, T. Takagi, R. Yasuhara, K. Horiba, H. Kumigashira, M. Oshima, 2008 IEEE International Electron Devices Meeting (2008) 1-4.
- [5] A. Chen, M.-R. Lin, 2011 International Reliability Physics Symposium (2011) MY.7.1-MY.7.4.
- [6] W.G. Kim, M.G. Sung, S.J. Kim, J.Y. Kim, J.W. Moon, S.J. Yoon, J.N. Kim, B.G. Gyun, T.W. Kim, C.H. Kim, J.Y. Byun, W. Kim, T.O. Youn, J.H. Yoo, J.W. Oh, H.J. Kim, M.S. Joo, J.S. Roh, S.K. Park, 2010 Proceedings of the European Solid State Device Research Conference (2010) 400-403.
- [7] S. Tirano, L. Perniola, J. Buckley, J. Cluzel, V. Jousseume, C. Muller, D. Deleruyelle, B.D. Salvo, G. Reimbold, *Microelectronic Engineering* 88 (2011) 1129-1132.
- [8] C. Cagli et al., *Techn. Digest of 2011 International Electron Devices Meeting*, pp. 28.7.1, 2011

- [9] M. Bocquet, D. Deleruyelle, C. Muller, J.-M. Portal, *Applied Physics Letters* 98 (2011) 263507.
- [10] U. Russo, D. Ielmini, C. Cagli, a. L. Lacaita, S. Spiga, C. Wiemer, M. Perego, M. Fanciulli, 2007 IEEE International Electron Devices Meeting (2007) 775-778.
- [11] B. Gao, S. Yu, N. Xu, L.F. Liu, B. Sun, X.Y. Liu, R.Q. Han, J.F. Kang, B. Yu, Y.Y. Wang, 2008 IEEE International Electron Devices Meeting (2008) 1-4.
- [12] C. Cagli, F. Nardi, D. Ielmini, *IEEE Transactions on Electron Devices* 56 (2009) 1712-1720.

Figure 1
[Click here to download high resolution image](#)

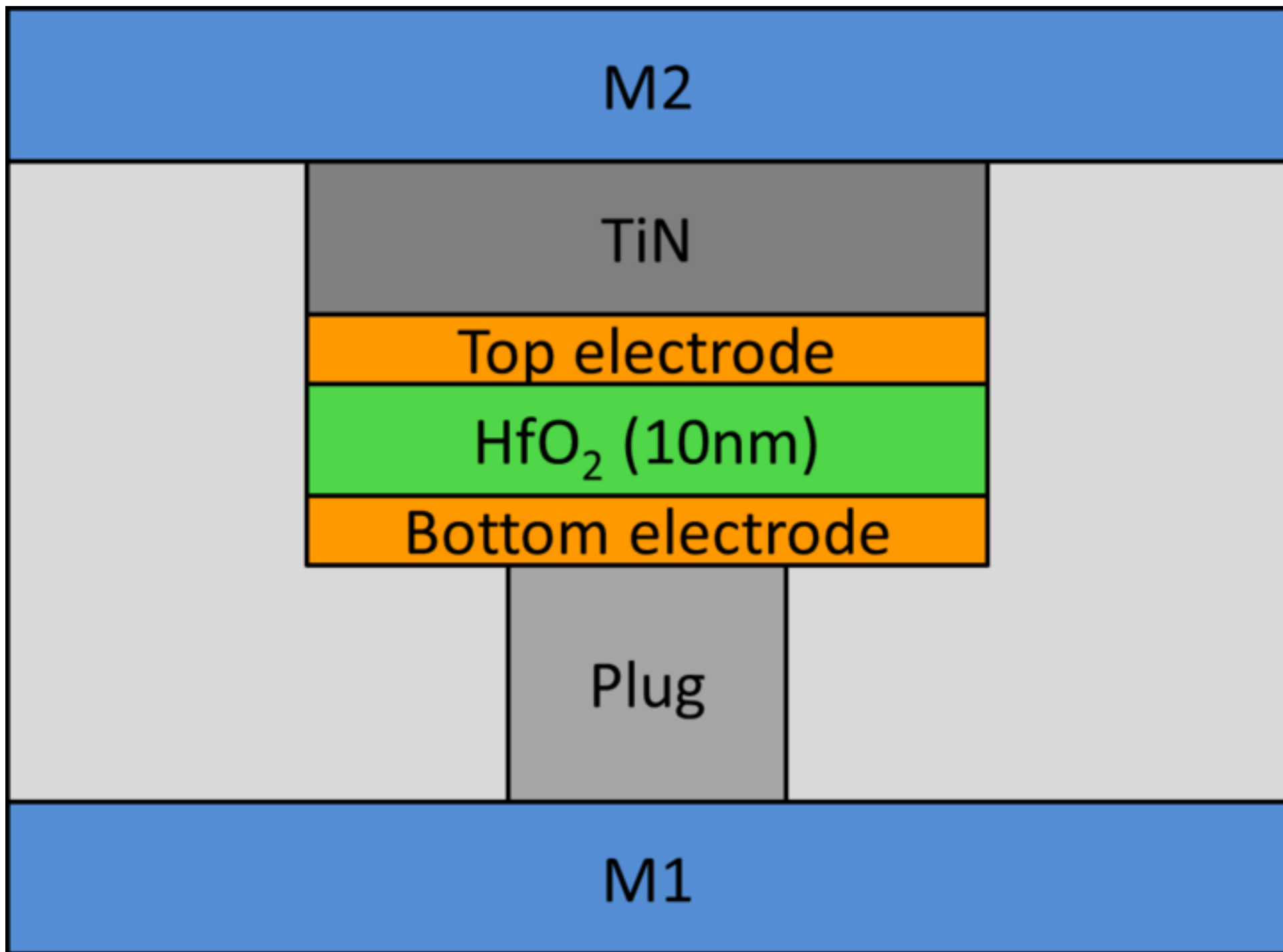


Figure 2a
[Click here to download Figures \(if any\): Figure2a.eps](#)

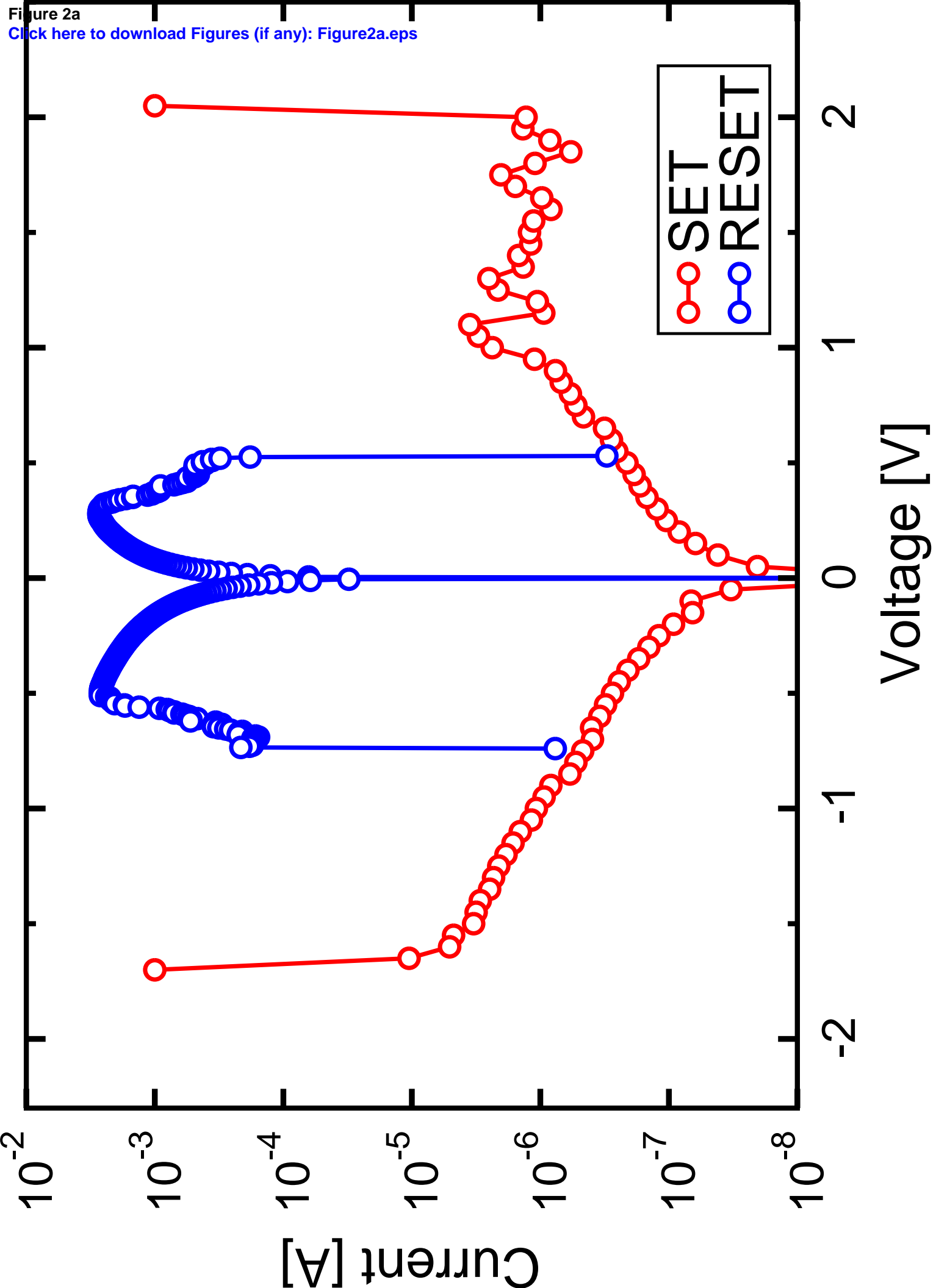


Figure 2b
[Click here to download Figures \(if any\): Figure2b.eps](#)

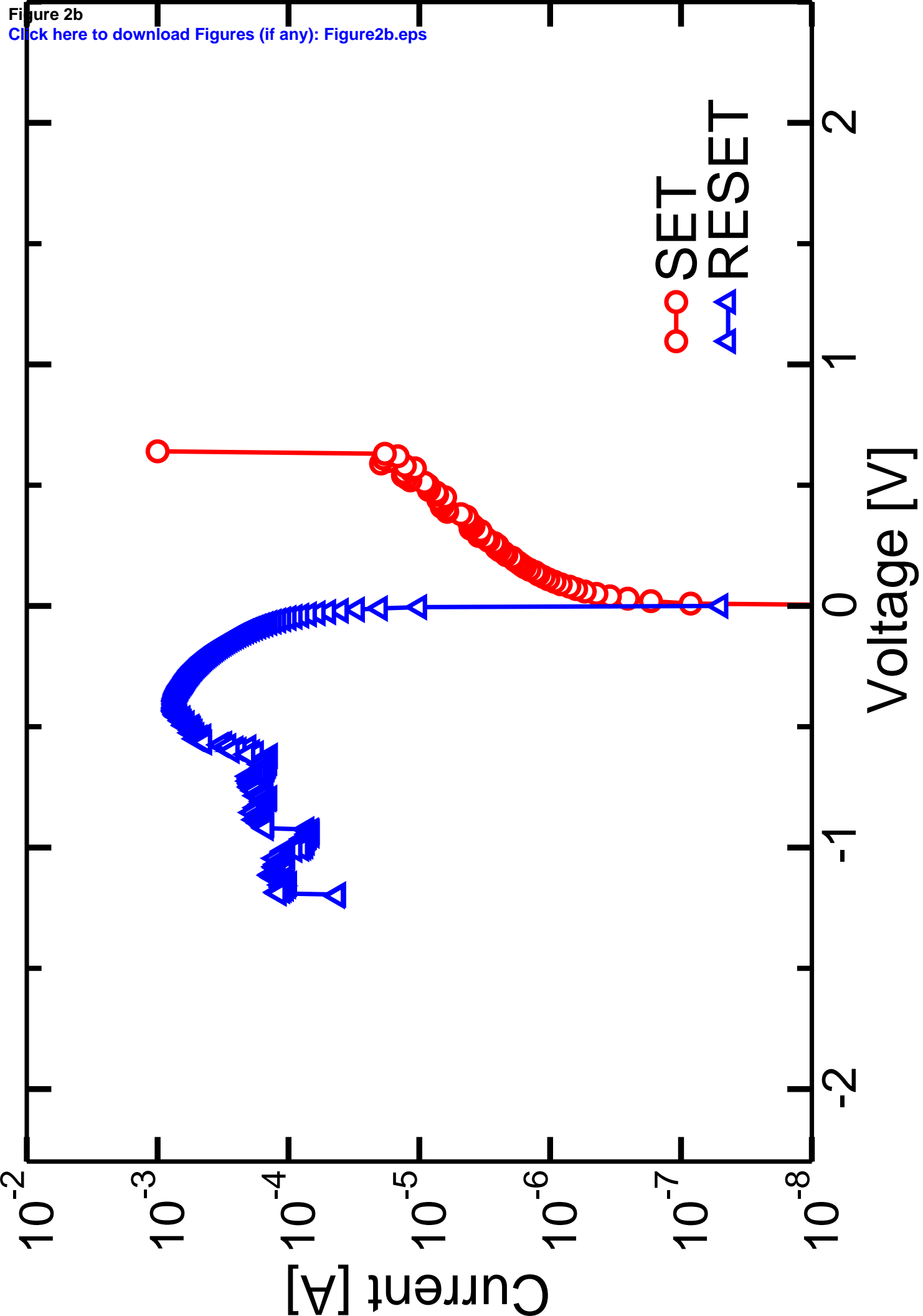


Figure 3a

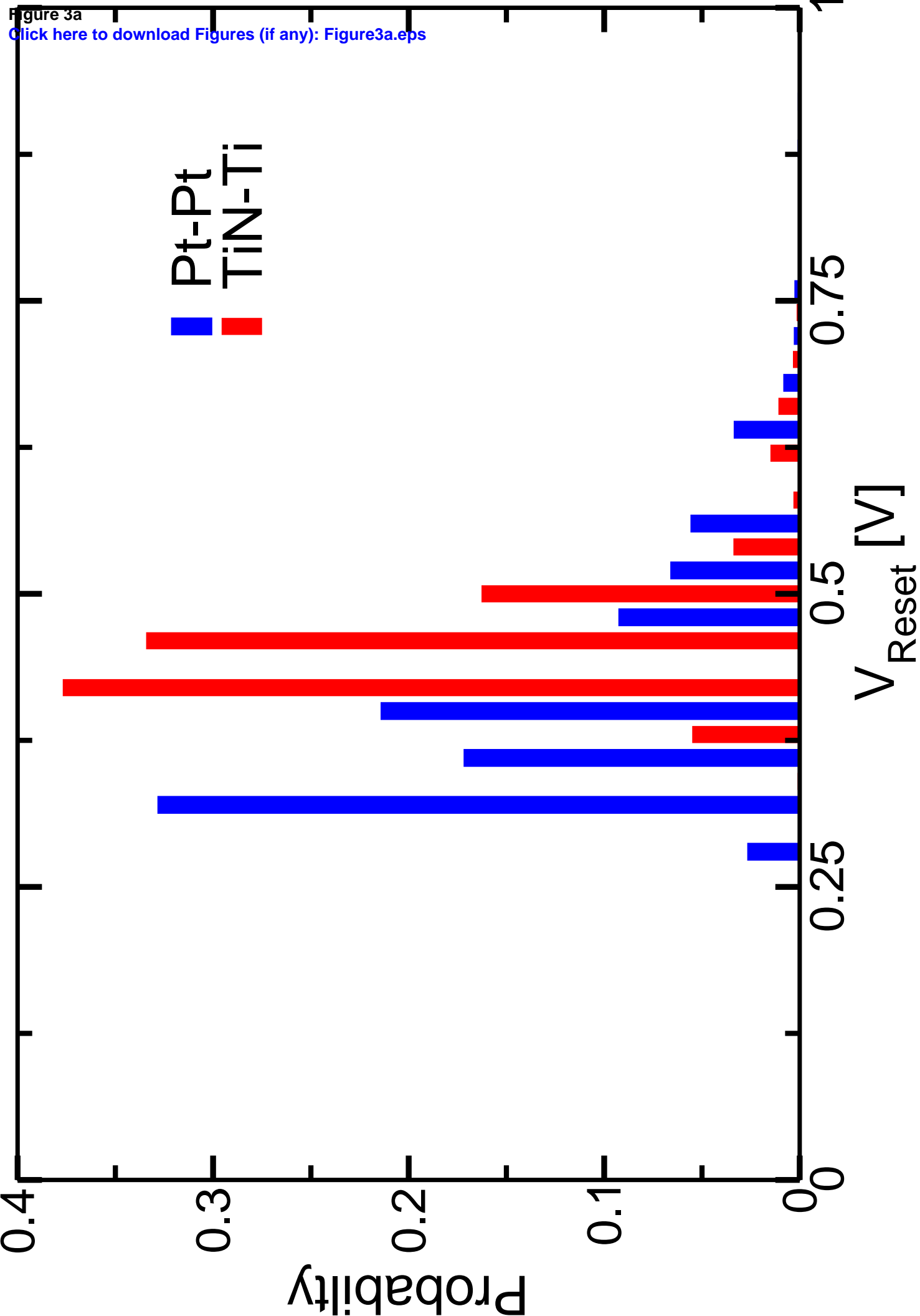
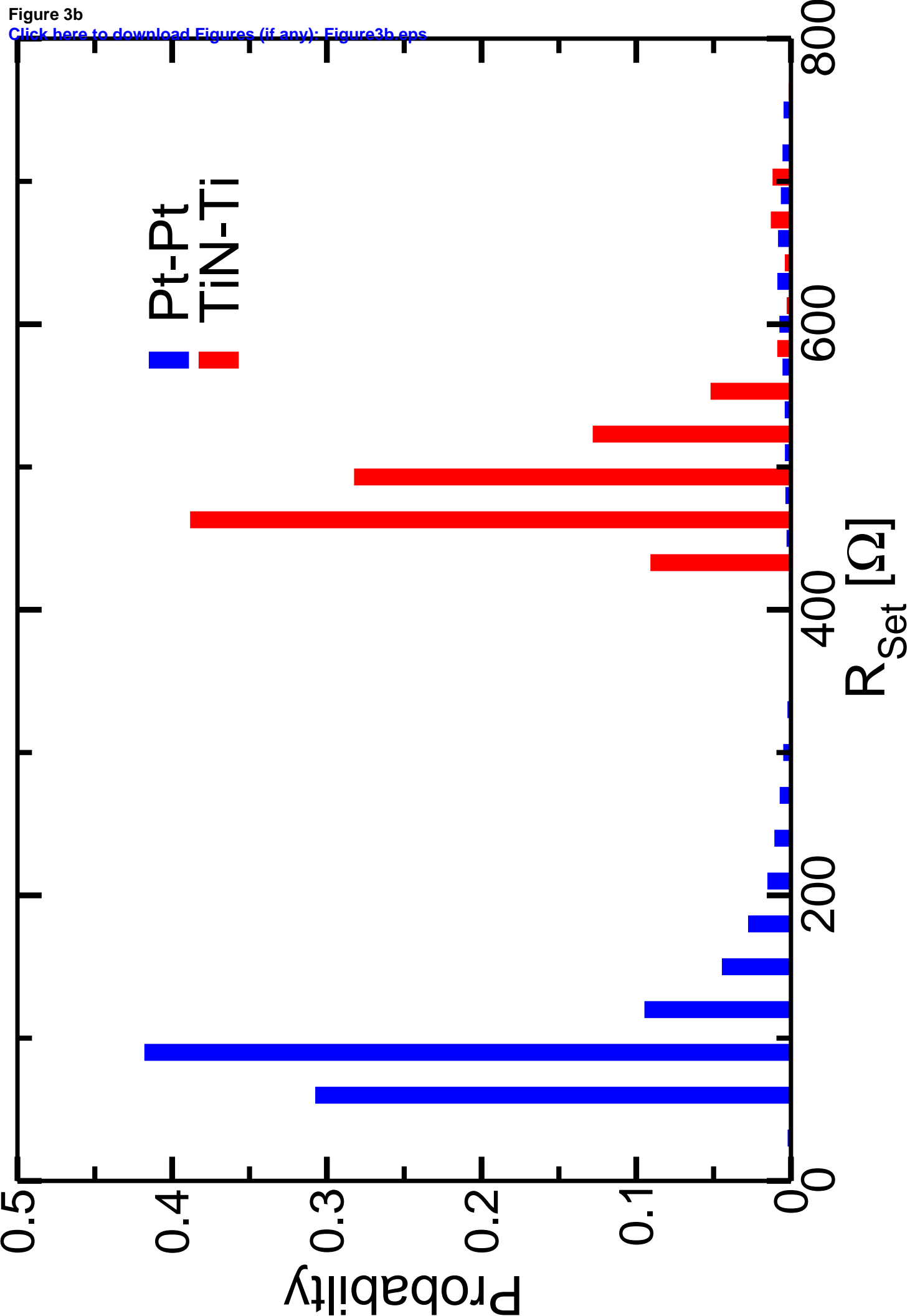
[Click here to download Figures \(if any\): Figure3a.eps](#)

Figure 3b

[Click here to download Figures \(if any\): Figure3b.eps](#)



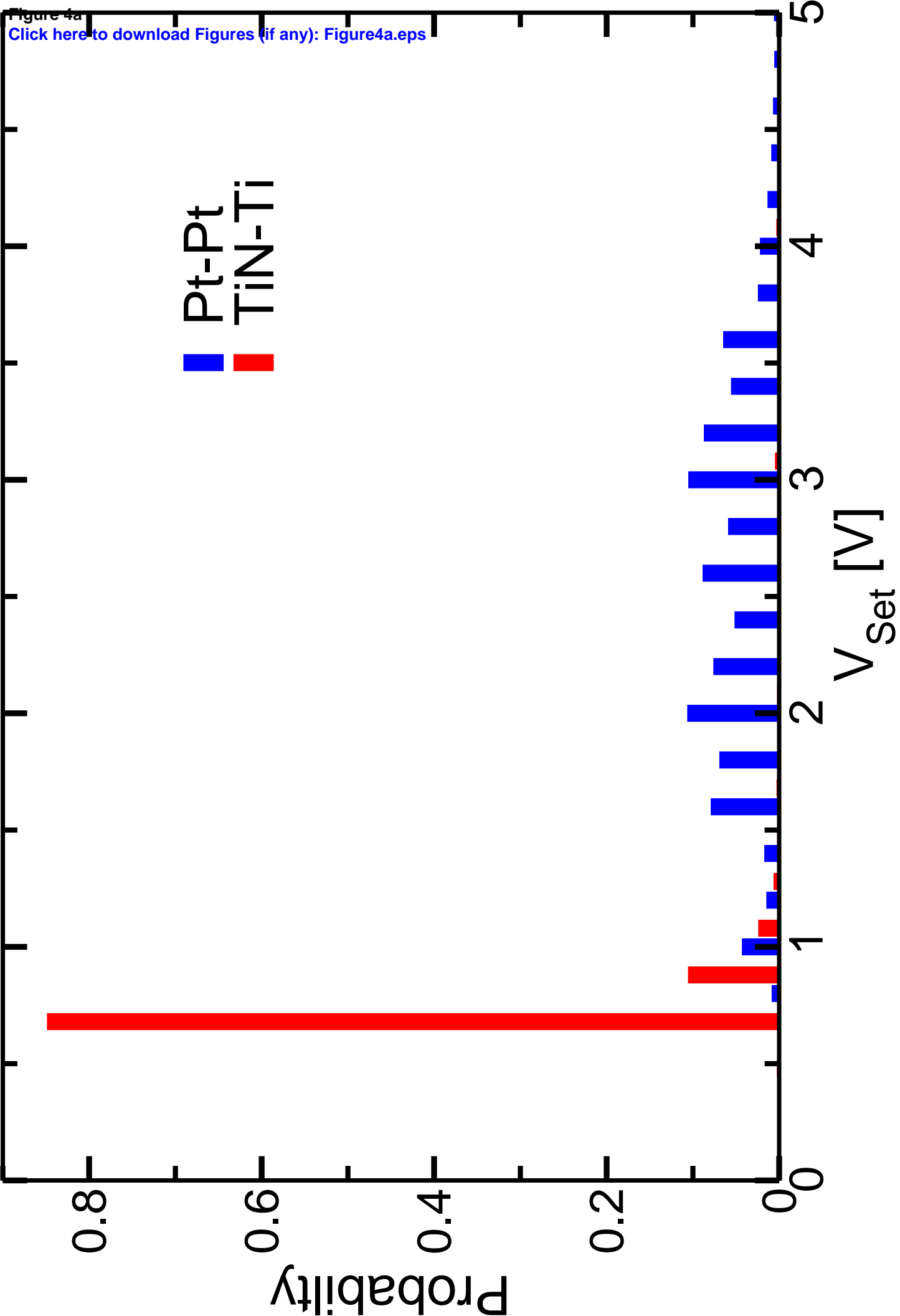


Figure 4b

[Click here to download Figures \(if any\): Figure4b.eps](#)

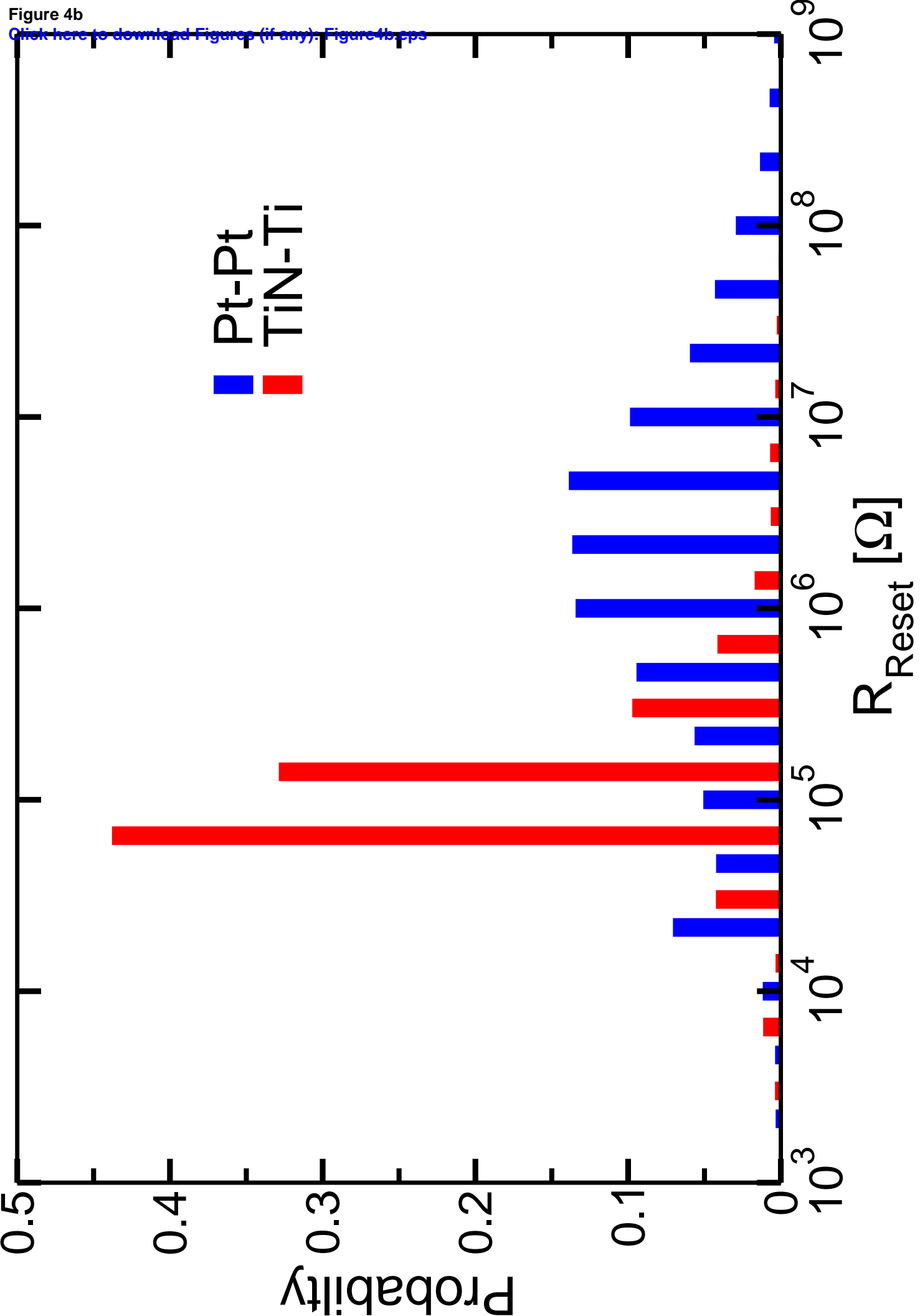
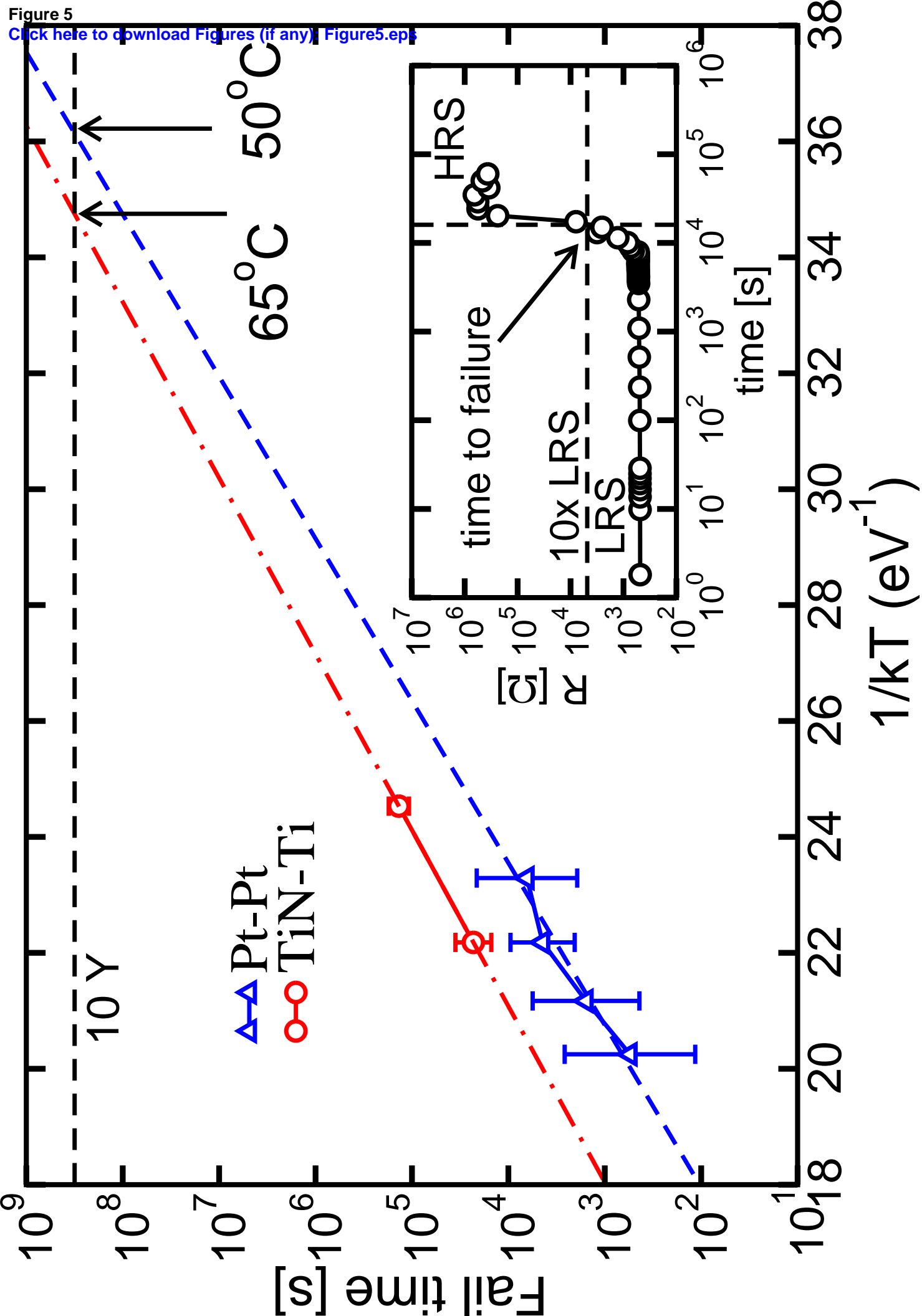


Figure 5

[Click here to download Figures \(if any\): Figure5.eps](#)



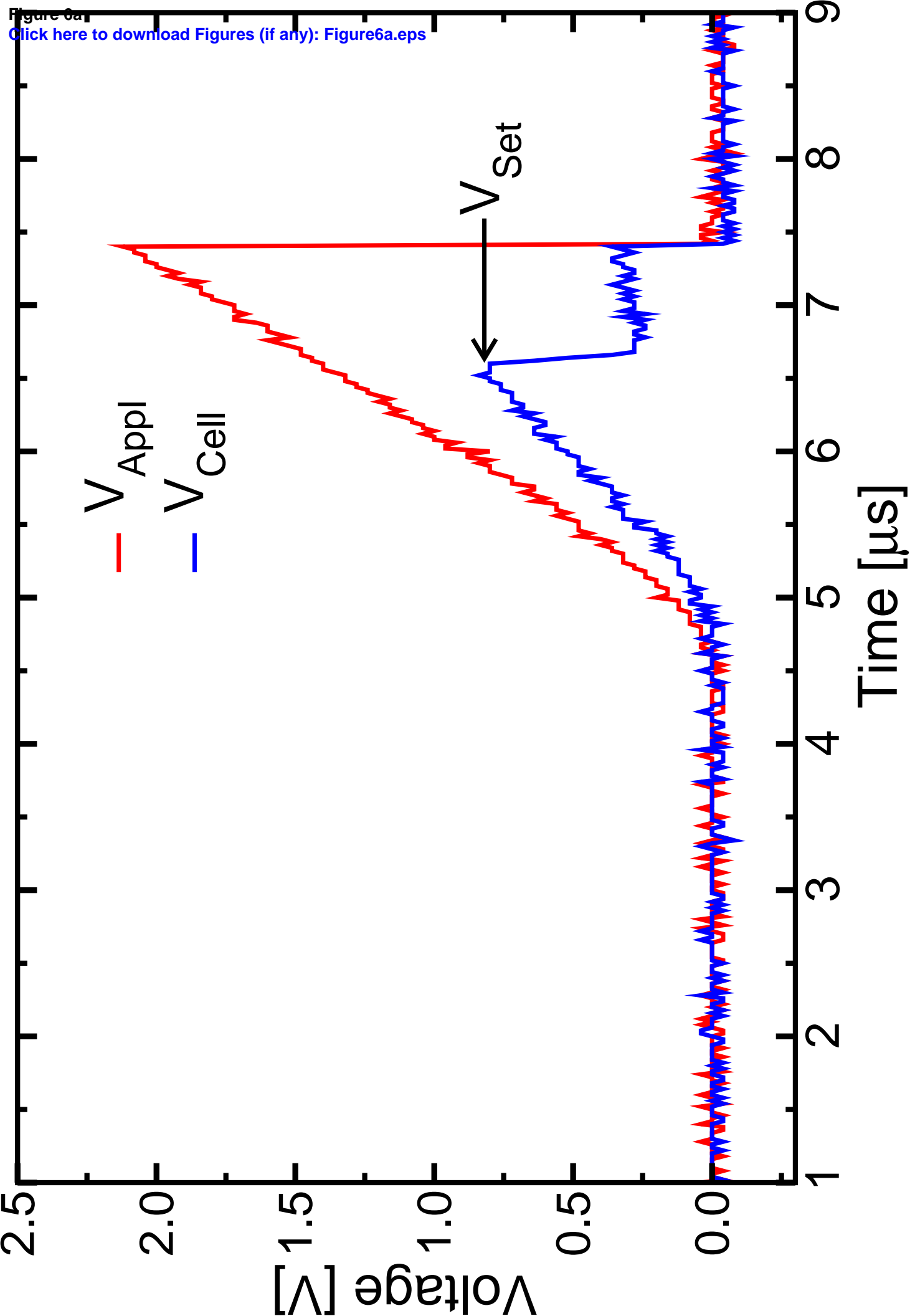


Figure 6b
[Click here to download Figures \(if any\): Figure6b.eps](#)

